Exploring the Carbon/Electrolyte Interface in Supercapacitors Operating in Highly Concentrated Aqueous Electrolytes

Cyrille Neto, Hien Pham, Rachelle Omnée, Aurélien Canizarès, Aneta Slodczyk, Michael Deschamps, Encarnacion Raymundo-Piñero

Exploring the Carbon/Electrolyte Interface in Supercapacitors Operating in Highly Concentrated Aqueous Electrolytes

Cyrille Neto,[1,2] *Hien T. T. Pham,*[1,2] *Rachelle Omnée,*[1,2] *Aurélien Canizarès,*[1] *Aneta Slodczyk,*[1,3] *Michael Deschamps,**[1,2] *Encarnacion Raymundo-Piñero**[1,2]

[1] CNRS, CEMHTI UPR3079, Univ. Orléans, 1D avenue de la Recherche Scientfique, 45071, Orléans, France

[2] Réseau sur le Stockage Électrochimique de l'Énergie (RS2E), FR CNRS 3459, 80039 Amiens Cedex, France

[3] Institut des Sciences de la Terre d'Orléans, CNRS/Université d'Orléans/BRGM, 1A Rue de la Ferollerie, 45071, Orléans, France

*Corresponding authors

Corresponding authors: raymundo@cnrs-orleans.fr, michael.deschamps@cnrs-orleans.fr

ABSTRACT: The development of superconcentrated or water-in-salt electrolytes (WISEs) has paved a new way toward realizing environmentally friendly, nonflammable batteries and supercapacitors based on aqueous electrolytes. The development of new electrolytes, such as WISEs, needs to be accompanied by further studies of the charging mechanism. This is essential to guide the choice of the electrode/electrolyte pairs for optimizing the performance of WISE-based supercapacitors. Therefore, to optimize the performance of carbon/carbon supercapacitors when using new, superconcentrated electrolytes, we present a detailed investigation of the carbon/electrolyte interface by combining electrochemical measurements with Raman and NMR spectroscopy and mass spectrometry. In particular, NMR provides crucial information about the local environment of electrolyte ions inside the carbon pores of the electrode. The results show that the structure of the electrolyte strongly depends on the concentration of the electrolyte and affects the mechanism of charge storage at the positive and negative electrodes.

KEYWORDS: *highly concentrated electrolytes, water-in-salt electrolytes, electrode/electrolyte interface, aqueous supercapacitors, carbon/carbon supercapacitors, charge storage mechanism, electrolyte structures, concentration effect*

Corresponding authors: raymundo@cnrs-orleans.fr, michael.deschamps@cnrs-orleans.fr

1. INTRODUCTION

The interest of the materials science community in highly concentrated aqueous electrolytes for energy storage systems (also called water-in-salt electrolytes (WISEs)) has been continuously raised since the work presented by Suo et al. in 2015.[1] In WISEs, the amount of water is not sufficient to complete the hydration sphere of the ions. Suo's pioneering work on a WISE composed of LiTFSI in water with a molality of 21 mol kg^{-1} showed the possibility of operating over a wide electrochemical stability window -ESW- with aqueous electrolytes. The small number of water molecules surrounding the ions widens the thermodynamic potential window, which is usually limited by water electrolysis.

In recent years, a number of studies have been devoted to determining the structure of TFSI-ion-based WISEs to advance the understanding of their electrochemical performance in energy storage systems, mainly in batteries. Experimental techniques such as infrared (IR), Raman and nuclear magnetic resonance (NMR) spectroscopy combined with molecular dynamics (MD) simulations have been used to explore ion/ion and ion/water interactions and to build a model for the structure of such WISEs.[1–4] The results show that when the concentration of LiTFSI increases, the hydrogen bonds in the water are replaced by water/ion interactions. At low LiTFSI concentrations, the ions slightly disrupt the structure of the water hydrogen bond network, whereas at high concentrations, the network is mainly composed of ion/water and ion/ion interactions. In short, for the case of LiTFSI at low concentrations, water molecules surround Li^+ ions, while $TFSI^-$ anions never come into close contact with Li^+ ions. Therefore, the electrolyte contains both “free” water molecules and solvated ions with small ion-ion interactions. As soon as the WIS regime is reached, almost all the water molecules solvate the Li^+ ions; thus, almost no free water remains, and the $TFSI^-$ anions coordinate with the Li^+ to form ionic aggregates, also called contact ion pairs (CIPs). Therefore, by increasing the concentration, the solvation structure of LiTFSI is changed and

Corresponding authors: raymundo@cnrs-orleans.fr, michael.deschamps@cnrs-orleans.fr

ion-ion interactions are promoted. This particular structuration will have consequences for the physico-chemical and electrochemical properties of a WISE. Primarily, the presence of little or no free water is the main reason for the extension of the electrochemical stability window (ESW) toward the thermodynamic limits of water electrolysis. This is a common feature for all WISEs, but for the particular case of LiTFSI, the fact that $TFSI^-$ anions are strongly coordinated to Li^+ cations leads to the cathodic decomposition of $TFSI^-$ and the formation of a solid electrolyte interface (SEI) over the negative electrode, which also helps to increase the ESW.[1] Another physico-chemical property impacted by the structure of WISEs that has a great influence on the electrochemical performance is the conductivity. For LiTFSI-based electrolytes, the maximum ionic conductivity is obtained at a concentration of 3.5 mol kg^{-1} as a compromise between viscosity and the number of ionic carriers is reached.[5] Increasing the concentration leads to a decrease in the ionic conductivity, reaching approximately 8 mS cm^{-1} at 21 mol kg^{-1}, which is close to the value observed for nonaqueous electrolytes. Such values limit the use of LiTFSI-based WISEs below room temperature.[6] In addition to the disadvantages presented above, LiTFSI has a high toxicity and a very high cost, which will not be negligible due to the high concentrations used in WISEs.[7]

To overcome these drawbacks, research is progressing in different directions.[6,8] The following directions have been proposed in the literature to increase the conductivity: decreasing the concentration of the WISE, preparing mixtures with organic solutions or optimization of the salt.[8] The problem of reduced conductivity at low temperatures can be reduced by using a mixture of organic solvents.[9] The introduction of cosolvents, therefore, is a priority direction; however, it has some negative impact on the electrochemical performance, and the operating mechanisms are not yet clear.[8] Finally, to reduce the cost of the electrolytes, some studies have presented WISEs based on low-cost salts containing alkaline cations and anions such as nitrate, perchlorate or acetate.[7,10–12] All the alternatives mentioned above

Corresponding authors: raymundo@cnrs-orleans.fr, michael.deschamps@cnrs-orleans.fr

present a large ESW: the use of either organic cosolvents, different salts or salt mixtures leads to a wider ESW than that for water.[8]

For the particular case of supercapacitors, WISEs have been less explored compared to batteries. As in the case of batteries, for carbon/carbon supercapacitors, LiTFSI is the most widely studied WISE, and cell voltages between 2.2 V - 2.4 V have been reported.[1–4] Other salts, such as $NaClO_4$,[7] $NaNO_3$,[10] CsF[11] or CH_3COOK,[12] have been more seldom presented in the literature, showing performances not far from those obtained with LiTFSI. From previous results reported in the field of carbon/carbon supercapacitors, it is clear that the charging mechanism depends on both the carbon electrode material and the electrolyte.[13–18]This implies that the development of new WISEs needs to be accompanied by further studies on the charging mechanism. This is essential to guide the choice of the electrode/electrolyte pairs for optimizing the performance of WISE-based supercapacitors.

Because of the novelty of WISEs, there are very few studies in the literature concerning charge storage mechanisms. Since the structure and physico-chemical properties of WISEs are different from those of dilute electrolytes, the electrical double layer is expected to be different.[6] Furthermore, the ion/water interactions are not homogeneous since, as discussed above for the LiTFSI-based WISE, water mainly solvates cations and not anions.[5] Due to their structure, it is common to compare WISEs with ionic liquids, so it would be interesting to apply the knowledge for the double layer at the ionic liquid/electrode interface to better understand the double layer at the WISE/electrode interface. Ionic liquids can contain polar/apolar domains that extend over a few nanometers.[19] Indeed, the small amount of water contained in these liquids remains around the anions, forming hydrogen bonds and creating anion-rich zones. For the case of WISEs, they also feature large areas that are either rich in anions or rich in cations inside the charged electrodes.[20] The number of anion–anion or cation–anion pairs increases for high ion concentrations, and an interconnected ion-rich

Corresponding authors: raymundo@cnrs-orleans.fr, michael.deschamps@cnrs-orleans.fr

network appears.[21,22] However, even though the concentration of ions in WISEs is very high, water molecules are also present in relatively large numbers. Miyazaki et al.[23] showed that in the water-in-salt regime, clusters of water molecules are observed 99% of the time. These clusters do not exceed five water molecules in size and are mostly composed of clusters with 1 or 2 molecules. These clusters behave energetically like single water molecules. Therefore, it is difficult to reduce them to hydrogen. Li et al.[24] showed by molecular dynamics simulations that water molecules in WISEs are strongly bound in the ion solvation sphere. LiTFSI is located around the lithium ions and does not affect the capacitance variation for the supercapacitor. In summary, all the work done thus far through different simulations shows that WISEs are mainly composed of self-assembled nanostructures with strong ion-ion interactions. This leads to the formation of large cation- or anion-rich domains on the electrode surface upon charging the supercapacitor. All these theoretical works on the formation of a double layer in supercapacitors with carbons in WISEs provide a basis for a further understanding of the charging mechanisms. However, more experimental studies are needed to support the simulations and advance the understanding of these systems.

Therefore, one of the objectives of this work is to explore the effect of the concentration of the electrolyte on the charging mechanism at the electrode/electrolyte interface of a carbon/carbon supercapacitor by combining electrochemical measurements with other experimental techniques, such as electrochemical pulsed mass spectrometry (PEMS) and NMR. In particular, we have focused on potassium acetate (KAc) as an aqueous electrolyte in carbon/carbon supercapacitors. Potassium acetate is a very cheap salt with a very high water solubility limit (27 mol kg^{-1} or a salt: water mass ratio of 1:2), so water-in-salt regimes can easily be achieved. KAc is seldom used as a WISE in carbon/carbon supercapacitors. A previous study has showed that the ESW for KAc is increased with electrolyte concentration and that a cell voltage of 2.0 V can be achieved in a carbon/carbon supercapacitor.[12] In

Corresponding authors: raymundo@cnrs-orleans.fr, michael.deschamps@cnrs-orleans.fr

addition to the environmental interest in a fluorine-free salt and its low cost, the choice of KAc is driven by the fact that we can easily explore the charging/discharging mechanism for a carbon/carbon supercapacitor with NMR. In fact, water and acetate ions and their different chemical environments can easily be distinguished by ^{1}H NMR spectroscopy. The new insights obtained for the–charge storage mechanism will provide valuable information for optimizing supercapacitors through the point of view of the system configuration and the carbon electrode choice.

2. EXPERIMENTAL SECTION

The electrolytes were prepared from KAc salt (99% pure, Sigma–Aldrich) with a molality ranging from 1 mol kg^{-1} to 25 mol kg^{-1}. As KAc is a highly hygroscopic salt, some precautions were taken for obtaining the targeted concentrations with maximum accuracy. First, the salt was stored and weighed in a glove box before placing into a bottle closed by a septum. The desired amount of ultrapure water was injected by using a syringe outside of the glove box. After stirring overnight, the electrolyte was bubbled by a flow of neutral gas to eliminate the dissolved oxygen. The pH and conductivity of the KAc-based electrolytes were measured using a pH meter-conductivity meter (METTLER).

Electrolytes with different concentrations were analyzed by Raman spectroscopy. The Raman spectra were recorded at room temperature using a Renishaw InVia Qontor Raman microspectrometer. A 514 nm excitation laser line was focused onto each liquid sample through a long working distance 50X objective (Leica, 0.5 N.A.). The low laser power was adapted to avoid undesirable water/solution evaporation. As the liquid is transparent, the focusing point was chosen to be 20 µm below the surface to avoid any loss of signal due to sample evaporation. The backscattering Raman signal was analyzed by a Raman spectrometer (1800 lines/mm grating, Renishaw Centrus CCD Camera). Prior to any measurement, the

Corresponding authors: raymundo@cnrs-orleans.fr, michael.deschamps@cnrs-orleans.fr

spectrometer was calibrated using an internal silicon reference. Raman spectra were measured over a wide spectral range (500–4000 cm^{-1}). The acquisition time of 60 s allowed us to record the Raman spectrum with a very satisfactory signal-to-noise ratio.

Carbon electrodes were prepared by mixing 85 wt.% nanoporous carbon (Carbon A, Norit (Cabot) DLC Super 50 and Carbon B, CO_2 activated char), 5 wt.% carbon black (C65, Timcal, Switzerland) and 10 wt. % binder (polytetrafluoroethylene, PTFE or Teflon®, Sigma–Aldrich) in ethanol. The mixture was stirred at 77 °C to evaporate part of the ethanol. The resulting paste was roughly flattened to obtain a film with a thickness of approximately 200 μm and densified to a final thickness of ~180 μm by a rolling press. After that, the film was dried at 100 °C for a minimum of 12 h and then punched to obtain electrodes with a diameter of 1 cm.

The porous texture of the materials and electrodes was analyzed by N_2 adsorption at 77 K and by CO_2 sorption at 273 K (Quadrasorb, Quantachrome, USA). Prior to the measurements, the samples were outgassed at 120 °C for 12 h under vacuum. The specific surface area was determined from the N_2 adsorption isotherm using the Brunauer−Emmett−Teller (BET) equation. The microporous volumes were determined by applying the Dubinin−Radushkevich method to the CO_2 adsorption data. The mesopore volume and the pore size distribution were determined by the 2D-nonlocal density functional theory (2D-NLDFT) method with a slit-shaped pore model applied to the N_2 adsorption data.

The surface functionality of the carbon-based electrodes was analyzed by temperature-programmed desorption (TPD) under an inert Ar atmosphere. The sample (10-15 mg) was heated under an Ar flow of 100 mL min^{-1} up to 1100 °C at a constant rate of 10 °C min^{-1}. The weight loss and the gas decomposition products were analyzed by using a thermobalance coupled to a mass spectrometer (MS, Skymmer, Neszch, Germany).

To investigate the evolution of the porous texture and surface chemistry upon aging,

Corresponding authors: raymundo@cnrs-orleans.fr, michael.deschamps@cnrs-orleans.fr

the electrodes were removed from the supercapacitor cell, washed for 8 h by gentle stirring with distilled water to remove electrolyte ions, vacuum filtered five times with distilled water and then finally dried in an oven at 110 °C for 12 h. Fresh electrodes were also subjected to the same treatment for comparison.

Electrochemical characterization was performed with two- and three-electrode Swagelok® cells by cyclic voltammetry (2 mV s^{-1} for two electrode cells and 5 mV s^{-1} for three electrode cells), galvanostatic charge/discharge (0.2 to 10 A g^{-1}), voltage floating and impedance spectroscopy by using MPG-2 and VMP3 multichannel potentiostats/galvanostats (Biologic, France). Two-electrode Teflon Swagelok® cells were assembled with carbon electrodes over gold current collectors, and glass fiber paper (Whatman®, thickness 670 µm) was used as a separator. An Ag/AgCl reference electrode was added to the two-electrode Teflon Swagelok® cells for performing standard three-electrode cell investigations over one of the carbon electrodes (using the other carbon electrode as the counter electrode) or for monitoring electrode potentials during two-electrode cell operation. The outgassed electrolyte was retrieved through the septum by using a syringe and rapidly introduced into the electrochemical cell to minimize contact with the ambient air.

The gases evolved during aging for a symmetric carbon/carbon supercapacitor by voltage floating were monitored operando by pulsed electrochemical mass spectrometry (PEMS)[25] using a custom airtight and compact electrochemical cell with large electrodes (20 cm^2). Different valves and flowmeters were synchronized to the potentiostat/galvanostat (SP-50, Biologic, France) using software developed in-house for transporting the gases to a mass spectrometer (Skymmer, Netzsch, Germany) at the desired moment during the cell operation. Prior to the aging of the supercapacitor, the electrodes were conditioned by a series of galvanostatic charge–discharge cycles at a current density of 0.5 A g^{-1} for a gradually increasing voltage from 1.0 V to 1.8 V (5 cycles at each stage). After conditioning, the cell

Corresponding authors: raymundo@cnrs-orleans.fr, michael.deschamps@cnrs-orleans.fr

was held at a cell voltage of 1.8 V for 50 h for accelerated aging (or floating experiment). Every hour, five galvanostatic charge/discharge cycles (0.5 A g^{-1}) were performed for capacitance and resistance measurements, while the gaseous products accumulated inside the cell were swept to the mass spectrometer (MS) at the same time for analysis.

^{1}H magic angle spinning nuclear magnetic resonance (MAS-NMR) was used not only to characterize electrolytes but also to study the charge storage mechanism. For this purpose, two different kinds of experiments were performed. The first one consists of polarizing the carbon in a three-electrode cell, in the presence of the electrolyte, from the potential of zero charge of carbon (pzc) either positively (with values higher than pzc) or negatively (with values smaller than pzc). The zero charge potential is the potential at which the electrode is neither positively nor negatively charged, and it was recorded immediately after the electrode was wetted with the electrolyte. For the case of KAc at 1 mol kg^{-1} and 25 mol kg^{-1}, the pzc values were measured to be -0.2 and -0.3 V vs. Ag/AgCl, respectively. For every targeted potential, a new electrochemical cell was built. The second one was used for monitoring the electrodes at different states of charge of the supercapacitor. For this, a symmetric carbon/carbon cell was conditioned by gradually charging-discharging the cell voltage up to the desired value and then holding this voltage for 15 minutes. In each case, the electrode was extracted from the electrochemical cell and placed into a sealed insert made of Kel-F® inside a ZrO_2 rotor with an external diameter of 4 mm. Bruker 4 mm MAS double resonance ^{1}H-X probes were used. NMR experiments were performed using Bruker Avance spectrometers operating at a magnetic field of 7 T (300 MHz for ^{1}H). The rotor spins at the magic angle (54.7°) to average over the anisotropic interactions at a speed of 5 kHz. For all the ^{1}H NMR spectra, the homogeneity of the spectrometer was optimized with shimming coils, and the chemical shifts were referenced with the free water peak observed at 4.8 ppm. The spectra were fitted with Lorentzian and Gaussian using the dmfit program,[26] the baseline was

Corresponding authors: raymundo@cnrs-orleans.fr, michael.deschamps@cnrs-orleans.fr

corrected, and the areas for each fitted contribution, which are proportional to the amount of ^{1}H spins in the sample, were used to calculate the relative concentrations of water and acetate inside and outside the pores of the carbon electrode.

3. RESULTS AND DISCUSSION

3.1. Electrochemical characterization

Figure 1a shows the electrochemical performance of porous carbon A with KAc-based electrolytes with concentrations ranging between 1 and 25 mol kg^{-1}. The figure confirms that the concentration has a great influence on the ESW of the electrolyte when using porous carbons as electrodes, as observed with the use of Pt electrodes by Tian et al.[8] By increasing the concentration, the oxidation potential does not change much, probably because the oxidation of the carbon material occurs at a lower potential than that of the electrolyte as it will be further explored by operando gas analysis. On the other hand, the electrolyte concentration has a remarkable effect on the reduction potential during negative polarization. The potential for H_2 gas evolution is lower when the electrolyte concentration is higher. Moreover, increasing the electrolyte concentration favors the contribution of redox reactions related to hydrogen storage as they appear when decreasing the potential under the value of water reduction (-1.26 V vs. Ag/AgCl for the KAc at 25 mol kg^{-1}).[25,27–31] Such behavior will have a great impact on the maximum cell voltage up to which the supercapacitor will be able to operate.

To determine the maximum cell voltage, Figure 1b shows the charge efficiency and capacitance of carbon/carbon supercapacitors built with KAc electrolytes obtained at different cell voltages. The figure shows that the capacitance increases with the cell voltage for all electrolytes. These results indicate that by increasing the cell voltage, the electrodes operate in a potential range where pseudofaradaic reactions increasingly occur along with the formation

Corresponding authors: raymundo@cnrs-orleans.fr, michael.deschamps@cnrs-orleans.fr

of the electric double layer (EDL), both contributing to the capacitance. In that sense, the efficiency obtained for each cell voltage will be an indication of the reversibility of these reactions. Figure 1b shows efficiency values for almost 100% in all electrolytes for a cell voltage of lower than 1.5 V. However, for higher cell voltages, there is a clear effect of the concentration: the degradation in the efficiency with the cell voltage decreases with the electrolyte concentration. Therefore, such results confirm the interest in increasing the concentration of the electrolyte to achieve a higher cell voltage and improving the energy density and efficiency.

The results presented above can be explained by monitoring the potentials of the electrodes during the operation of the cell by introducing a reference electrode into the symmetric carbon/carbon supercapacitor. Figure 1c shows the potentials of the positive and negative electrodes (E^+ and E^-, respectively) at the cell voltage indicated on the horizontal axis and the potential obtained after discharging the cell to 0.0 V (E_{0V}). At lower concentrations, when increasing the cell voltage, the positive electrodes rapidly reach the potential values where the carbon materials can be oxidized (see the ESW presented in Figure 1). Increasing the electrolyte concentration leads to a decrease in the electrode potentials, which enables both electrodes to operate inside the ESW for the electrode/electrolyte up to higher cell voltages. Therefore, the decrease in the potential of the positive electrode at higher concentrations can explain the results shown in Figure 1b. The faster degradation of the efficiency with the cell voltage observed at lower concentrations is related to the irreversible oxidation of the carbon at the positive electrode. Therefore, as has been previously observed for other aqueous electrolytes,[25,27–29] the positive electrode is considered to be the limiting electrode that determines the cell voltage.

In conclusion, increasing the electrolyte concentration lowers the electrode potential during the operation of the cell and prevents the oxidation of the positive electrode. On the

Corresponding authors: raymundo@cnrs-orleans.fr, michael.deschamps@cnrs-orleans.fr

other hand, the increase in the H_2 evolution overpotential at negative polarization at high concentrations (Figure 1) prevents the irreversible reduction of water at the negative electrode. As a result, supercapacitors using highly concentrated WISEs are able to safely operate at higher cell voltages compared to their counterparts using diluted electrolytes. For the case of KAc at a concentration of 25 mol kg^{-1} (Figure 1b), the supercapacitor can operate at a cell voltage of 2.0-2.2 V. However, aging experiments are needed to more accurately assess the maximum operating cell voltage.

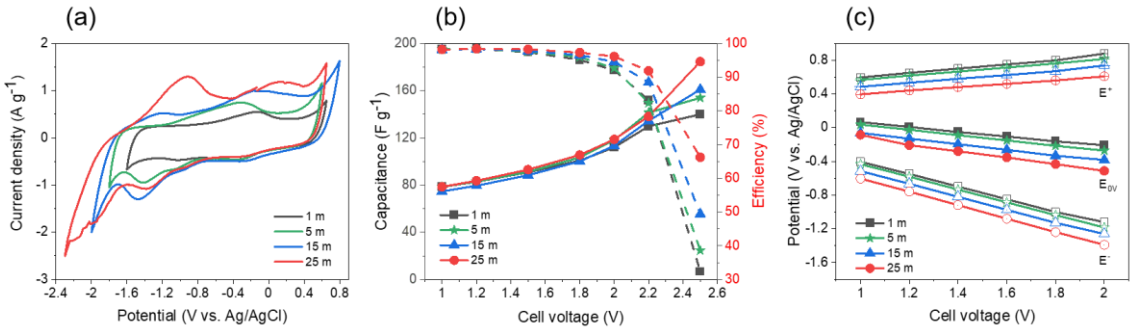

Figure 1. (a) Cyclic voltammetry curves measured at a scan rate of 5 mV s^{-1} for KAc electrolytes at different concentrations over a porous carbon electrode. (b) Capacitance and charge efficiency of symmetric carbon/carbon supercapacitors at different cell voltages with KAc at different concentrations. (c) Potentials of positive (E^+) and negative electrodes (E^-) at different cell voltages and their potentials when discharging the cells to 0.0 V (E_{0V}).

3.2. Accelerated aging of supercapacitors

Figure 2a shows the results obtained for accelerated aging experiments performed with a supercapacitor built using a 25 mol kg^{-1} WISE at various cell voltages. Accelerated aging involves charging the supercapacitor up to the targeted maximum cell voltage and then keeping the system at this potential. In this kind of experiment, so-called floating experiment, the capacitance of the system is measured from time to time to monitor the remaining capacitance as a function of the floating time, as presented in Figure 2. This floating

Corresponding authors: raymundo@cnrs-orleans.fr, michael.deschamps@cnrs-orleans.fr

experiment accelerates the aging because, in a typical galvanostatic charge/discharge experiment, the supercapacitor operates at maximum voltage values for a very short time, wherein irreversible reactions are most likely to occur. As an example, our WISE supercapacitor cell operating at 1.8 V stays between 1.75 and 1.80 V for just 12 s (from 218 s total discharge time) at a current density of 0.5 A g^{-1} and only 0.3 s (from 5.5 s total discharge time) if the current density is set to 10 A g^{-1}. Therefore, a 10-hour floating experiment corresponds to approximately 3000 cycles at 0.5 A g^{-1} or 120 000 cycles at 10 A g^{-1}. Thus, aging by galvanostatic charge/discharge for up to 1000-10000 cycles is not representative as an aging experiment to reliably determine the maximum cell voltage, especially if these cycles are performed at high current densities. Returning to the results presented in Figure 2a, as expected, increasing the cell voltage decreases the cycle life of the supercapacitor. The figure shows that 2.0 V is an acceptable cell voltage, as has already been shown in only one other report using KAc WISE in carbon/carbon supercapacitors.[9] In addition, Figure 2a shows that 1.8 V is a safer cell voltage, enabling extension of the cycle life by almost 3 times. Regarding the effect of the concentration of the electrolyte in the cycle life on the supercapacitor, Figure 2b shows that a working voltage of 1.8 V increasing the concentration up to 25 mol kg^{-1} enables a doubling of the cycle life of the supercapacitor.

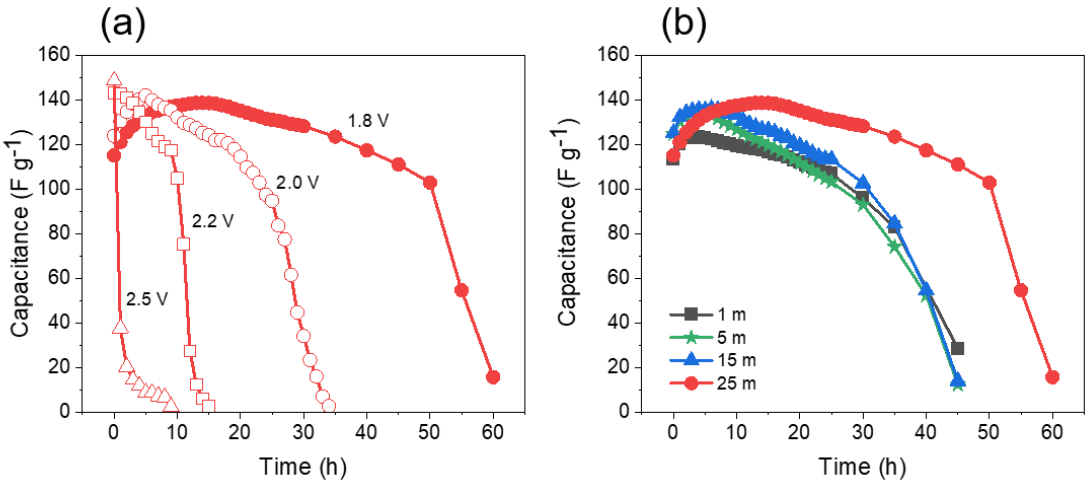

Figure 2. Capacitance as a function of the floating time of carbon/carbon supercapacitors (a)

Corresponding authors: raymundo@cnrs-orleans.fr, michael.deschamps@cnrs-orleans.fr

built with a 25 mol kg^{-1} KAc electrolyte operating at different cell voltages and (b) built with KAc electrolytes at different concentrations operating at 1.8 V.

To understand the origin of the capacitance loss during aging as a function of the concentration, we performed pulsed electrochemical mass spectrometry (PEMS). The PEMS method consists of accumulating the gases produced inside the supercapacitor cell every hour during floating at 1.8 V for subsequent introduction of short pulses of an inert gas through the cell to the MS. This approach enables minimization of gas dilution and increases the sensitivity for quantitative analysis of the gases produced at the electrode/electrolyte interface during supercapacitor operation.[25] When performing *operando* PEMS analysis during aging of the supercapacitors with KAc electrolyte at the lowest (1 mol kg^{-1}) and highest concentration (25 mol kg^{-1}), the main gases of H_2 and CO_2 were monitored (Figure 3a). H_2 evolution results from the reduction of water at the negative electrode, and CO_2 can be produced either by carbon oxidation or by acetate electrolysis at the positive electrode. Figure 3a shows that for the 1 mol kg^{-1} electrolyte, the amounts of H_2 and CO_2 produced rapidly increase up to a maximum value at approximately 25-30 h of floating and then decrease. However, for the 25 mol kg^{-1} electrolyte, there is a very small amount of CO_2 released (see inset of Figure 3a, where the Y-axis is divided by a factor of 100) and a small amount of H_2 is evolved. In addition to CO_2 and H_2, some gases related to acetate decomposition (CH_3, CH_2O, C_2H_6, etc.) are observed for the 1 mol kg^{-1} electrolyte but not for the 25 mol kg^{-1} electrolyte (see the example for a supercapacitor cell after 30 hours of floating shown in Figure S1). Such results are in concordance with the potentials reached at the positive and negative electrodes while aging the supercapacitor in different electrolytes, as shown in Figure 3b. For the 1 mol kg^{-1} electrolyte, considering the narrow stability potential window (Figure 1), both the positive and the negative electrodes operate at potentials where reactions take place in the

Corresponding authors: raymundo@cnrs-orleans.fr, michael.deschamps@cnrs-orleans.fr

electrode/electrolyte interface. For this electrolyte, when the number of hours of floating is increased, the maximum potential attained by the positive and negative electrodes continuously increases. Such a rise in the maximum potential at the positive electrode further promotes oxidation reactions, which can be expected to lead to an increase in CO_2 release. At the negative electrode, the increase in the potential during the first hours of floating is not sufficient to prevent the irreversible reduction of water, and H_2 is continuously released. At approximately 25-30 hours, the amounts of evolved CO_2 and H_2 decrease, while the maximum potential of the electrodes sharply increases. Therefore, the decrease in H_2 is easily understood as the electrode no longer operates out of its stability window, but the decrease in CO_2 shows the opposite behavior for the electrode potential evolution.

At this point, it is important to evoke that a variation in the operating potential window for an electrode during aging of a supercapacitor occurs to balance a capacitance variation to maintain the charge equivalence between the positive (q_+) and negative (q_-) electrodes:

$q_+ = q_-$ with q = mass × capacitance × potential range (Equation 1)

Therefore, for the 1 mol kg^{-1} electrolyte, the operating potential window of the positive electrode with floating time is observed to increase to compensate for the capacitance loss, as shown in Figure 3b. A postmortem analysis performed over the electrodes after 50 hours of aging (Figure 3c) confirms that oxidation of the carbon at the positive electrode occurs as the surface oxygen content is increased from 0.3 wt.% to 4.7 wt.%. This oxidation drives the decrease in the mass of the electrode and leads to a total collapse of the porosity, as the specific surface area of the electrode is decreased from 964 $m^2 g^{-1}$ to 10 $m^2 g^{-1}$ (Figure 3c). The decrease in the mass of the positive electrode leads to a decrease in the CO_2 evolution during the final hours of floating. On the other hand, the negative electrode suffers less during floating, as the specific surface area does not decrease much and the oxygen content does not vary much. Therefore, the sudden loss of capacitance observed in Figure 2b is more related to

Corresponding authors: raymundo@cnrs-orleans.fr, michael.deschamps@cnrs-orleans.fr

the oxidation of the positive electrode, resulting in a decrease in its specific surface area and its ability to store ions, as already observed for other diluted aqueous electrolytes.[5–10]

For the 25 mol kg^{-1} electrolyte, as the potentials are shifted down and the potential stability window is larger (Figure 1a), almost no gas is evolved during the first few hours of floating. Variations in electrode potentials are observed at a later floating time and are not as important as for the 1 mol kg^{-1} electrolyte supercapacitor, resulting in a lower level of gas production. As a result, the oxidation of the positive electrode is considerably limited after 50 hours of floating. Figure 3c shows that the oxygen content is increased by only up to 2.6 wt.% for an approximately 20% decrease in the specific surface area. Nevertheless, such variations in the physico-chemical properties of the positive electrode are responsible for the decrease in the device capacitance observed after approximately 40 hours of aging, as deduced from Figure 3b from the increase in the operating voltage window. Hence, the decrease in capacitance of the system shown in Figure 2 for highly concentrated electrolytes is also a consequence of positive electrode degradation.

Corresponding authors: raymundo@cnrs-orleans.fr, michael.deschamps@cnrs-orleans.fr

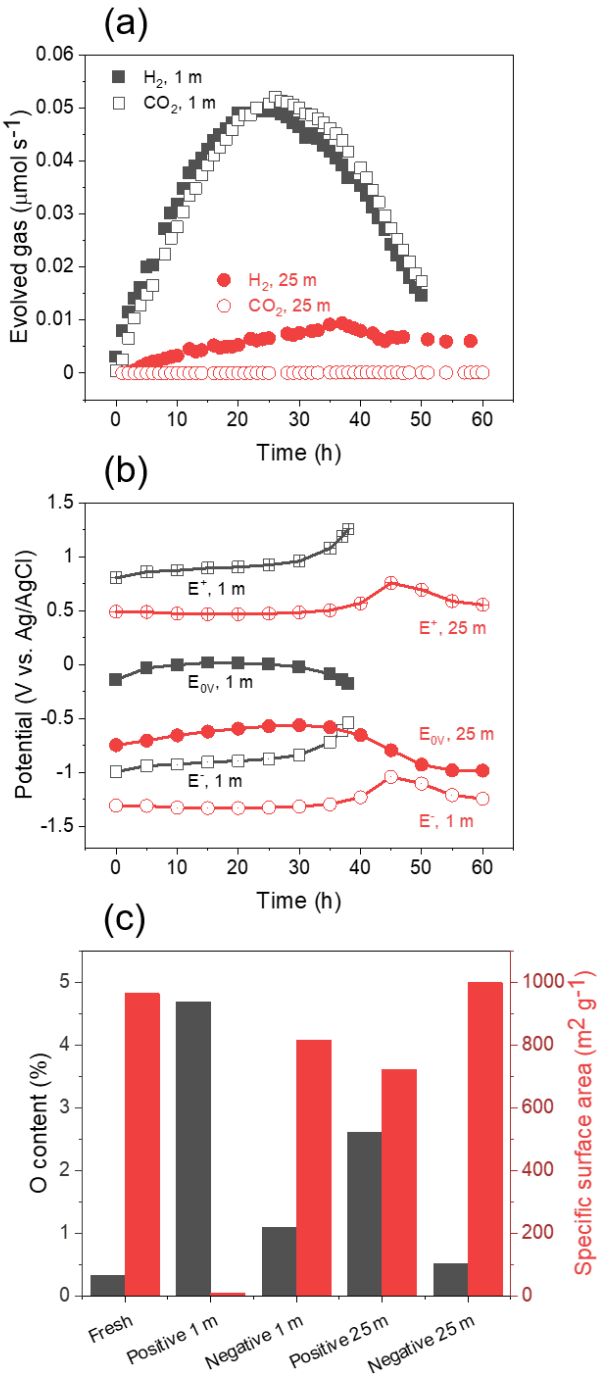

Figure 3. (a) H_2 and CO_2 produced at the electrode/electrolyte interfaces of carbon/carbon supercapacitors with AcK electrolytes at 1 mol kg^{-1} and 25 mol kg^{-1} while floating at 1.8 V. (b) Potentials of the positive (E^+) and negative electrodes (E^-) and their potentials when discharging the cells to 0.0 V (E_{0V}) as a function of floating time. (c) Surface oxygen content and specific surface area of the fresh electrodes obtained after 50 h of floating at 1.8 V.

Corresponding authors: raymundo@cnrs-orleans.fr, michael.deschamps@cnrs-orleans.fr

In conclusion, the main cause of aging in our dilute aqueous-based supercapacitors is the oxidation of the positive electrode. Two other causes include, first, the decomposition of the electrolyte, as deduced from the evolution of H_2 and CO_2 (Figure S1a), and second, the pressure increase inside the cell resulting from the evolution of all the gases from the electrode and electrolyte degradation (Figure S1c). Fortunately, increasing the concentration of the electrolyte decreases the oxidation of the positive electrode and the degradation of the electrolyte (Figure S1b). Reducing the extent of these irreversible reactions has an important influence on the cell pressure during aging (Figure S1c); however, the most important impact will be the possibility of operating the supercapacitor at a higher cell voltage to store more energy.

Moreover increasing the KAc concentration does not have an important effect on the charge capability of the supercapacitor (Figure S2a) and the performance in terms of power density outperforms the one obtained with a supercapacitor using a 21 m LiTFSI WISE operating at cell voltage of 2.4 V.[32] Although the maximum energy density that can be extracted are similar for a carbon/carbon supercapacitor using KAc 25 mol kg^{-1} or LiTFSI 21 mol kg^{-1} (19.7 Wh kg^{-1} and 19.0 Wh kg^{-1}, respectively), the energy density obtained at 10 s discharge time was as high as 8.5 Wh kg^{-1} for the AcK while only 5.3 Wh kg-1 can be extracted for the LiTFSI (see Ragone plot presented as Figure S2b).

3.3 Optimizing the system by an asymmetric mass configuration

The results presented above provide valuable information for optimizing the system. Even for the electrolyte with the highest concentration, the positive electrode operates at a potential in which it is oxidized upon aging. Figure 4a shows that at the cell voltage of 1.8 V, the positive electrode operates at a potential slightly out of the stability window of the carbon in this electrolyte (see Figure 1a) while the negative one stays at a potential far from the

Corresponding authors: raymundo@cnrs-orleans.fr, michael.deschamps@cnrs-orleans.fr

negative polarization limit. Therefore, the total stability potential window of the carbon presented in Figure 1a is not very well used. In addition, increasing the concentration of the electrolyte leads to an asymmetry of the system in terms of the capacitance of the positive and negative electrodes: a slight increase in the capacitance of the negative electrode but a significant decrease in the capacitance of the positive electrode (see Figure 4b and Figure S3 for symmetric supercapacitors operated at 1.8 V and 1.0 V, respectively). Such an asymmetry on the capacitance of the electrodes will become the origin of the asymmetry in the operating potentials shown in Figure 4a. The operating potential of the positive electrode is therefore needed to be decreased in order to improve the cell voltage and the operating life of the supercapacitor. It can be deduced from Equation 1 that the potential range of the positive electrode will decrease if the mass of the positive electrode increase, for maintaining the equivalence of charge stored at the positive and negative electrodes (assuming that the specific capacitance of the electrodes does not change). Considering that at the cell voltage of 1.8 V the capacitance of the negative electrode is 1.5 times higher than that of the positive one (Figure 4b), we doubled the mass of the positive electrode, firstly to compensate the capacitance difference and secondly to further increase the operating potential window of the negative electrode (as its potential was far from the limit found in Figure 1). Figure 4a shows that assembling an asymmetric cell with a positive electrode mass that is 2 times larger than that of the negative electrode enables the positive electrode to operate in a narrower potential range than that of the symmetric system. Consequently, this leads to a lower maximum operating potential and extends the cycle life: the cycle life of a cell operating at 1.8 V is tripled, and that for a cell operating at 2.0 V is doubled (Figure 4c and d). However, increasing the mass of the positive electrode implies a decrease in the specific capacitance of the system. In fact, as shown in Figure 4b, the capacitance of the positive electrode is much lower than the capacitance of the negative electrode. This means that for supercapacitors with

Corresponding authors: raymundo@cnrs-orleans.fr, michael.deschamps@cnrs-orleans.fr

an electrolyte concentration of 25 mol kg^{-1}, increasing the mass of the positive electrode leads to a smaller specific capacitance with a negative impact on the capacitance of the system.

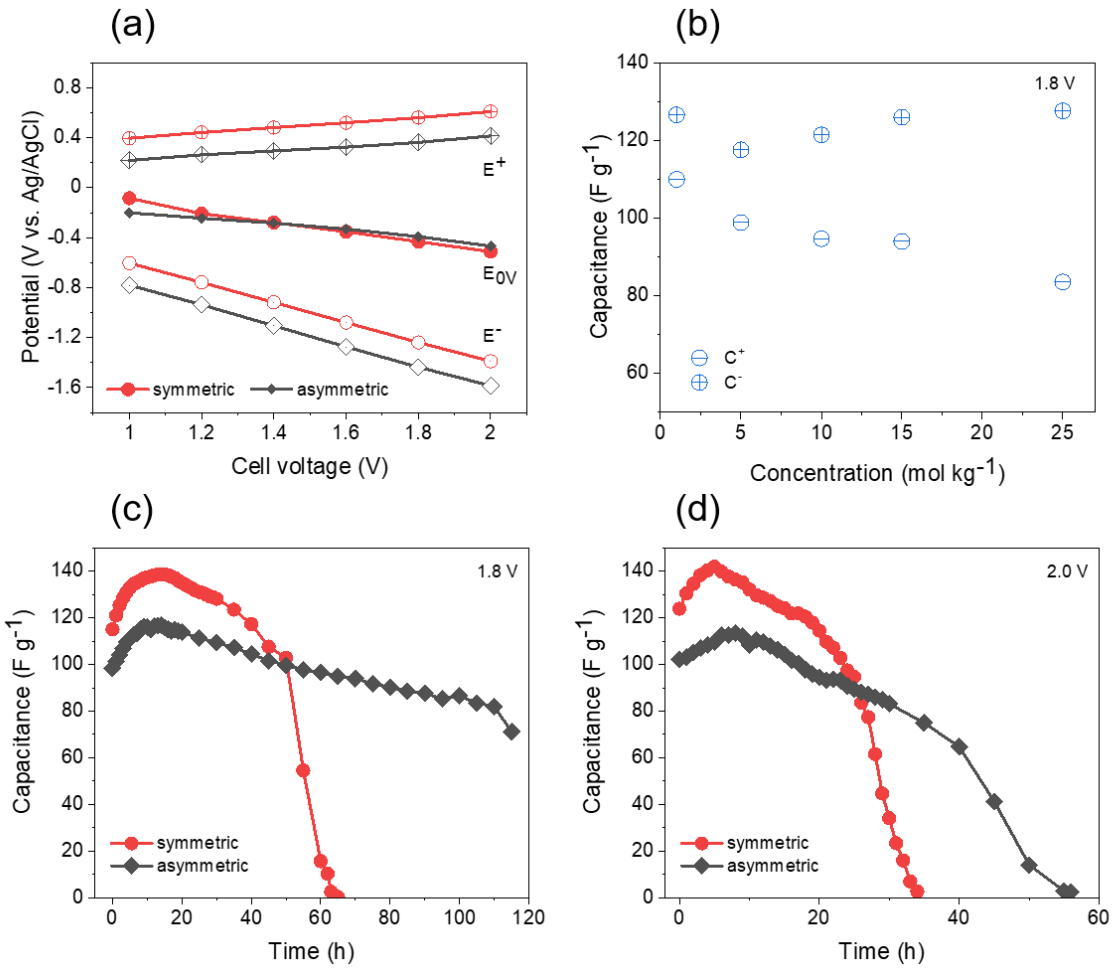

Figure 4. (a) Potentials of the positive (E^+) and negative electrodes (E^-) and their potentials when discharging the cells to 0.0 V (E_{0V}). (b) Specific capacitance of the positive and negative electrodes of symmetric supercapacitors with KAc electrolytes at different concentrations operating at 1.8 V. (c, d) The capacitance of asymmetric and symmetric supercapacitors operating at 1.8 V (c) and 2.0 V (d) as a function of floating time.

Corresponding authors: raymundo@cnrs-orleans.fr, michael.deschamps@cnrs-orleans.fr

3.4 Electrode/electrolyte interface characterization for determining charge storage mechanisms

To further optimize the operation of supercapacitors with concentrated electrolytes, it is necessary to gain more insight and knowledge into the phenomena arising at the electrode/electrolyte interface during operation. For this purpose, the effect of electrolyte concentration on ion/water organization inside the pores of the electrodes was investigated by ^{1}H solid-state NMR. ^{1}H solid-state NMR enables one to monitor acetate ions and water (Figure S4a) and to determine the relative amounts of each species in the bulk electrolyte or inside the carbon pores (Figure S4b). Actually, inside the carbon porosity, the electrolyte species (ions/solvent) experience the effect of neighboring ring currents created by the graphene-like sheets of the carbon material. The resulting local magnetic susceptibility results in a diamagnetic shift of the resonances of approximately -6/-7 ppm, as shown in Figure S4b, for the porous carbon A impregnated with 5 mol kg^{-1} KAc electrolyte. From the observed change in the shift, we can obtain information about the distance of the ^{1}H atoms of the methyl group of the acetate ion or that from the water molecule to carbon surface, and after fitting the spectra (as shown in Figure S4b), the relative concentrations of water and acetate inside and outside the pores can be quantified from the peak areas. After placing the carbon electrode into contact with the electrolyte and before polarization, i.e., at the point of zero charge (pzc), a shift of approximately 6 ppm for the acetate and for the water inside the pores is observed relative to the peak positions of the liquid electrolyte (Figure S4a), regardless of the electrolyte concentration. This indicates that the electrolyte ions immediately penetrate the carbon pores. The carbon electrode is then polarized either to potentials higher than pzc (positive polarization) or to potentials lower than pzc (negative polarization). Figure 5 shows the effect of polarization of the carbon electrode in a relatively diluted (5 mol kg^{-1}) and a highly concentrated (25 mol kg^{-1}) electrolyte on the relative concentrations of H_2O and acetate

Corresponding authors: raymundo@cnrs-orleans.fr, michael.deschamps@cnrs-orleans.fr

(calculated versus values at pzc) and their respective chemical shifts.

For the electrolyte at 5 mol kg^{-1} under positive polarization, Figure 5a shows that the relative concentration of acetate inside the pores increases followed by a further decrease. These results indicate that acetate ions enter the pores during polarization but that beyond ca. 0.4 V vs. Ag/AgCl, the acetate concentration decreases because of the decomposition of the electrolyte at the positive electrode, as shown by PEMS. Moreover, Figure 5b shows that the shift for the acetate sharply increases towards positive polarization, indicating a reorganization of the acetate ions in the porosity of the carbon electrode, with the COO^- group getting closer to the surface and the H of the methyl groups moving further away (ca. 1-2 Å away based on calculations[33]). It must be noted that a positive shift can result from changes in the electronic density on the carbon; however, such changes are expected to be independent from the observed electrolyte molecule and are expected to be of lower magnitude at such low voltage changes.[17] At the same time, Figure 5a shows that the concentration of adsorbed water remains almost constant during positive polarization, but it is difficult to quantify water in low-concentration solutions. However, Figure 5c shows that the ratio between water and acetate concentrations inside the porous carbon decreases during positive polarization, confirming that the acetate ions penetrate into the pores at the same time that the water-solvated K^+ ions leave. The increase in the water shift shown in Figure 5b supports the fact that H_2O is repulsed away from the charged carbon surface and leaves the porous carbon together with the K^+ ions. In summary, for positive polarizations, we have an ion exchange mechanism inside the carbon electrode.

At negative polarizations, with the 5 mol kg^{-1} electrolyte, the relative concentration of acetate inside the pores (relative to that at the pzc) decreases sharply with the potential (Figure 5a). These results indicate that the negatively charged acetate ions leave the pores during negative polarization. Moreover, Figure 5c shows that the ratio water/acetate largely increases

Corresponding authors: raymundo@cnrs-orleans.fr, michael.deschamps@cnrs-orleans.fr

to a higher extent than that for the case of positive polarization, indicating that in addition to ion exchange, with the acetate ions leaving the porous carbon and the K^+ ions entering together with a large solvation shell, co-ion expulsion probably also occurs. The relatively stable chemical shift observed for the water in Figure 5b confirms that water remains in the pores together with the K^+ ions since acetate ions leave. The decrease in the shift observed for the acetate ions indicates that the methyl group of the acetate ions remaining in the carbon pores will move closer to the electrode surface because only the anions neighboring the cations will remain behind, with COO^- groups located further away from the negatively charged carbon surface. In summary, we can say that for negative polarization, we have a mechanism between the ion exchange and the co-ion desorption.

Nevertheless, the picture is different when increasing the concentration of the electrolyte. For the electrolyte at 25 mol kg^{-1} under positive polarization, a small amount of acetate ions enters the carbon pores, while a small amount of water leaves, probably together with K^+ ions (Figure 5d). The small variation in the water and acetate shifts (Figure 5e) indicates that within positive polarization, a limited reorganization of moieties occurs inside the pores. The acetate ions remain close to the surface, and the water molecules solvating the K^+ ions are positioned slightly further away. These results indicate that instead of having an ion flux entering/leaving the porosity to form a double layer at the electrode/electrolyte interface consisting of solvated or partially desolvated ions of opposite sign for the polarized carbon surface, we now have large entities composed of anions, cations and solvent participating in the double layer.

Corresponding authors: raymundo@cnrs-orleans.fr, michael.deschamps@cnrs-orleans.fr

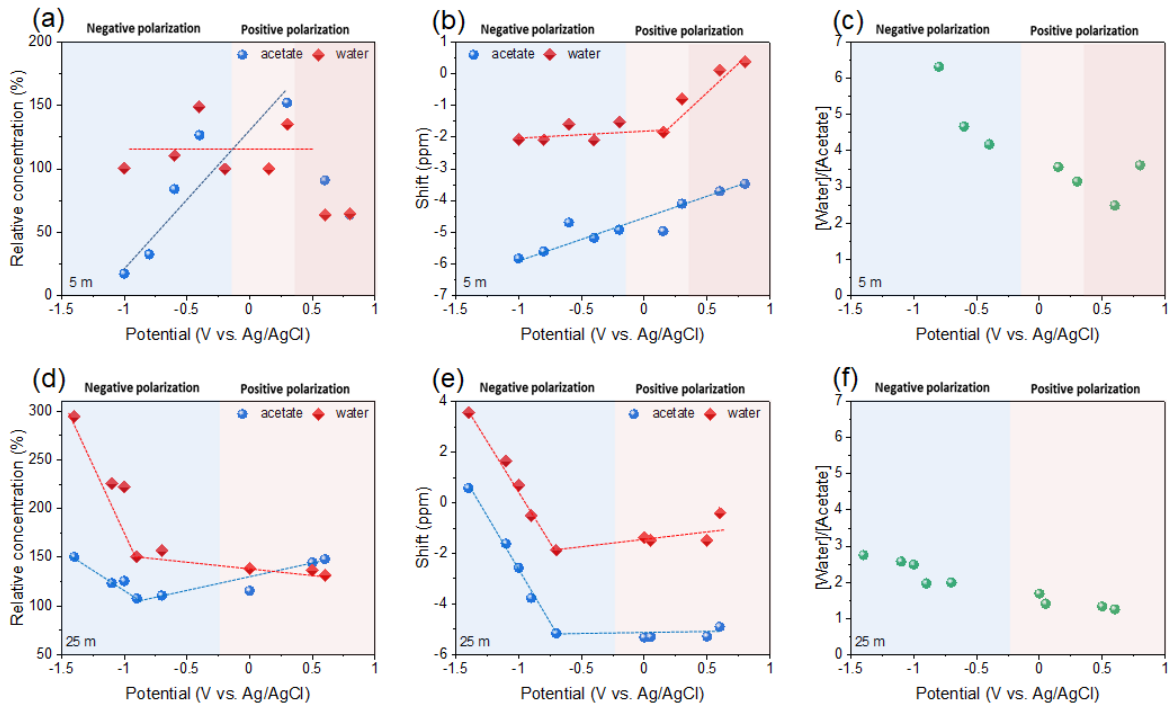

Figure 5. Calculated relative concentrations at different polarization potentials versus the values obtained at point of zero charge (a, d) for water and acetate ions inside the pores of the carbon electrode, their respective chemical shifts (b, e) and ratios for the amount of water to acetate ions obtained with KAc electrolytes of 1 mol kg^{-1} (a, b, c) and 25 mol kg^{-1} (d, e, f) obtained using ^{1}H solid-state NMR.

In fact, as determined by MD simulations,[34] in a diluted solution of KAc, K^+ is mainly solvated with water and well separated from the acetate anion by one or more hydration shells. In such a case, there are also large domains of free water. Increasing the electrolyte concentration leads to a transition from a conventional aqueous solution to an "ionic-liquid like" electrolyte. It has been reported that at a concentration of 25 mol kg^{-1}, free water molecules almost disappear as the water molecules become involved in the formation of bridges between separated ion pairs (SIP = K^+-(H_2O)-Ac^-), and contact ion pairs (CIP = K^+-Ac^-).

To obtain experimental information for the structure of the electrolyte, we conducted

Corresponding authors: raymundo@cnrs-orleans.fr, michael.deschamps@cnrs-orleans.fr

Raman spectroscopy. Figure 6a shows the Raman spectra measured for KAc solutions with concentrations ranging from 1 to 25 mol kg^{-1}. Among the different peaks, the most intense peaks are found for the C-C stretching at approximately 930 cm^{-1}, the CO stretching at approximately 1415 cm^{-1}, the CH_3 deformation at 1350 cm^{-1} and the water and CH_3 stretching bands above 3000 cm^{-1}. The figure shows that all bands are affected by an increase in electrolyte concentration. Note that according to previous literature, the C-C and C-O Raman bands appear to be especially concentration-sensitive.[35–38] As reported by Rudolph et al.,[35] direct contact of an acetate ion with a cation will result in a change in both the electronic structure of the ligated acetate and the force field, which will lead to a more pronounced change in its vibrational spectrum. For the particular case of acetates, Raman spectroscopy was used to reveal the presence of CIPs in concentrated aqueous solutions. For acetates with bivalent cations or with Li^+ ions, it has been observed that the formation of such CIP complexes, with a monodentate or bidentate interaction of the oxygen atoms and the cation, leads to the appearance of different shoulders in the υC-C and the υ_sC-O modes combined with their shift to higher wavenumbers.[35–37] The υC-C stretching mode and the υ_sC-O mode are depicted in Figure S5, while the concentration dependence for their peak positions and widths is presented in Figures 6b and 6c, respectively. It is clear that the effect of electrolyte concentration is not typical, as no shoulder appears, the peak widths increase very slightly and there is no shift to higher wavenumbers when increasing the concentration. In the absence of strong evidence for CIPs, the presence of a solvent shared ion pair is suggested, as reported in the literature for other concentrated solutions.[38] In fact, as has been previously reported,[38] the broadening of the C-C and C-O modes and their small shift to lower frequencies shown in Figures S5 and quantified in Figures 6b and c are consistent with a weak perturbation produced by the water-separated ion pair (SIP). In conclusion, in a 25 mol kg^{-1} solution of KAc with an ion/water ratio of 1:2.2, the species in the electrolyte are mostly structured as

Corresponding authors: raymundo@cnrs-orleans.fr, michael.deschamps@cnrs-orleans.fr

SIPs.

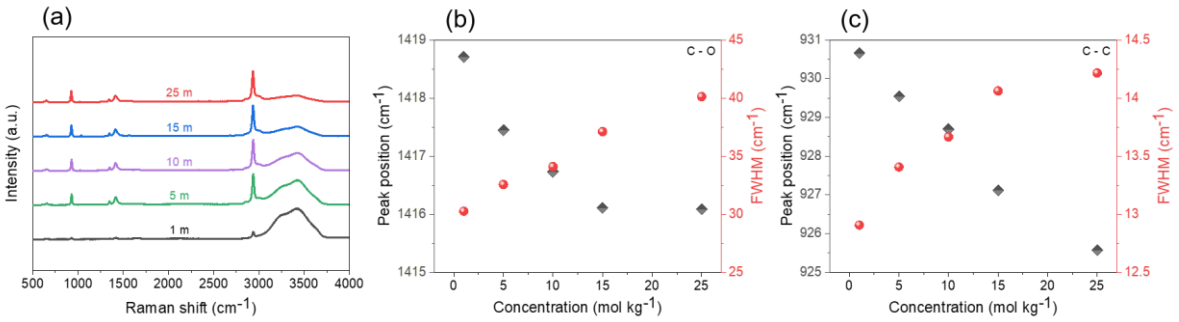

Figure 6. (a) Raman spectra measured for KAc solutions at different concentrations and the concentration dependence of the peak positions and widths of the υC-C mode (b) and υ_sC-O mode (c).

Therefore, we can now confirm that the mechanism for charging under positive polarization with the 25 mol kg^{-1} electrolyte consists of a reorientation of SIPs with the acetate moving closer to the polarized carbon surface. This kind of electrolyte structure also explains the NMR results obtained under negative polarization with the concentrated electrolyte. Figure 5d shows that, at the beginning of negative polarization, there is a slight decrease in the acetate ion concentration and a very small increase in the water concentration. This fact, coupled to the small shift observed in Figure 5e, indicates that at the beginning of negative polarization, some acetate ions leave the carbon pores, while some K^+ ions accompanied by water enter the pores. However, polarization not only further leads to a sharp increase in the water concentration but also to an increase in the relative concentration of acetate ions (Figure 5d). These results are in line with the fact that SIPs are involved in the charging mechanism instead of bare or solvated ions. Therefore, during negative polarization, SIPs enter the porous carbon upon polarization and are reoriented inside the pores with the K^+ ions located close to the surface and the acetate and water in a second and third layer, as

Corresponding authors: raymundo@cnrs-orleans.fr, michael.deschamps@cnrs-orleans.fr

reflected by the large positive chemical shift observed for the water and acetate ions (Figure 5e). Therefore, the charging mechanism at the negative electrode consists of a small ion exchange, probably implying that a small amount of K^+-water entities remains in the electrolyte (reflected also by the small variation of the water/acetate ratio presented in Figure 5f) followed by co-ion adsorption, as SIPs are the main species present in the electrolyte.

Finally, the differences in the charge storage mechanism for increasing electrolyte concentration are related to the different structures of the electrolyte itself. Such differences are depicted in Scheme 1.

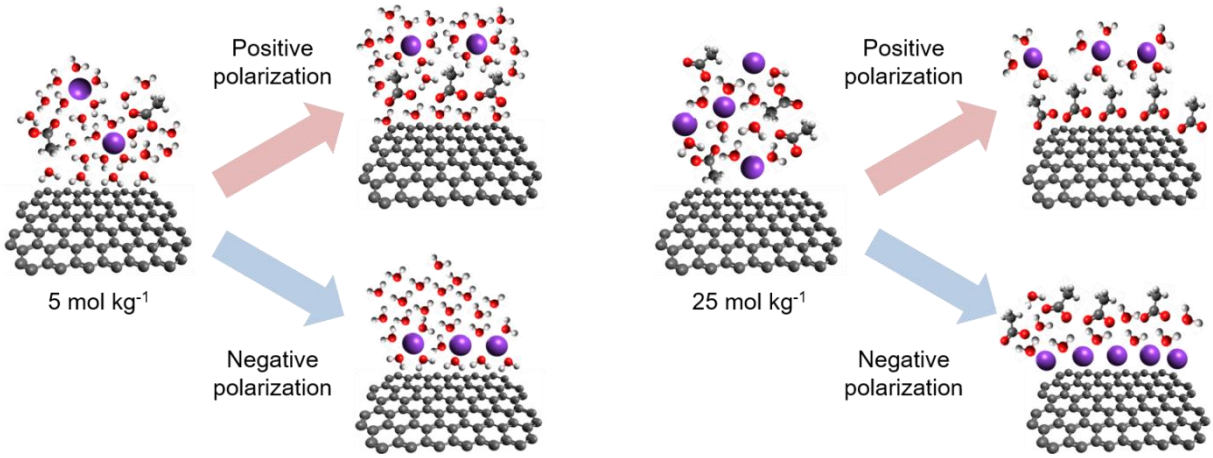

Scheme 1. Electrolyte structures and charge storage mechanisms at low and high electrolyte concentrations.

3.5. NMR characterization of ion fluxes during charge/discharge of the supercapacitor

The results presented above show that solid-state NMR spectroscopy provides valuable information about the charging mechanism for a carbon electrode with a very concentrated electrolyte. Moreover, NMR can be used to explore the fluxes of different moieties (ions, solvent, SIPs) during the charge–discharge cycle of a carbon–carbon symmetric supercapacitor. For this purpose, we conditioned the supercapacitor by charging/discharging up to a cell voltage of 1.0 V and then recorded the *ex situ* ^{1}H NMR spectra for the positive and

Corresponding authors: raymundo@cnrs-orleans.fr, michael.deschamps@cnrs-orleans.fr

negative electrodes as references to measure the relative concentrations of acetate and water ions at different states of charge and discharge inside the electrode pores (Figures 7 a and b). The chemical shifts for the adsorbed water and acetate were also extracted at each stage of cell charging for the positive and negative electrodes (Figures 7 c and d, respectively).

Regarding the relative amounts of water and acetate absorbed as a function of the cell voltage for the positive electrode (Figure 7a), if we observe only the charged state, we obtain similar results as shown in Figure 5d. In particular, the more we increase the cell voltage, the more acetate ions enter the pores, while the amount of water remains relatively constant until a cell voltage of 1.4 V is reached, following which the water amount increases for a cell voltage of 1.8 V. Similarly, if we look at the shifts inside the positive electrode during charging (Figure 7c), we obtain the same results as shown in Figure 5e. That is, when we increase the cell voltage from 1.0 V to 1.8 V, the shift for the acetate remains constant, while that for water is slightly increased. This indicates that during the charging process, especially when a certain voltage is exceeded, there is a slight exchange of ions with acetate ions entering the carbon pores. As discussed above, the results indicate that the charge mechanism mainly involves a reorganization of the species inside the pores during charging with acetate ions being placed with the COO^- side closer to the surface while water and K^+ ions remain further away.

Corresponding authors: raymundo@cnrs-orleans.fr, michael.deschamps@cnrs-orleans.fr

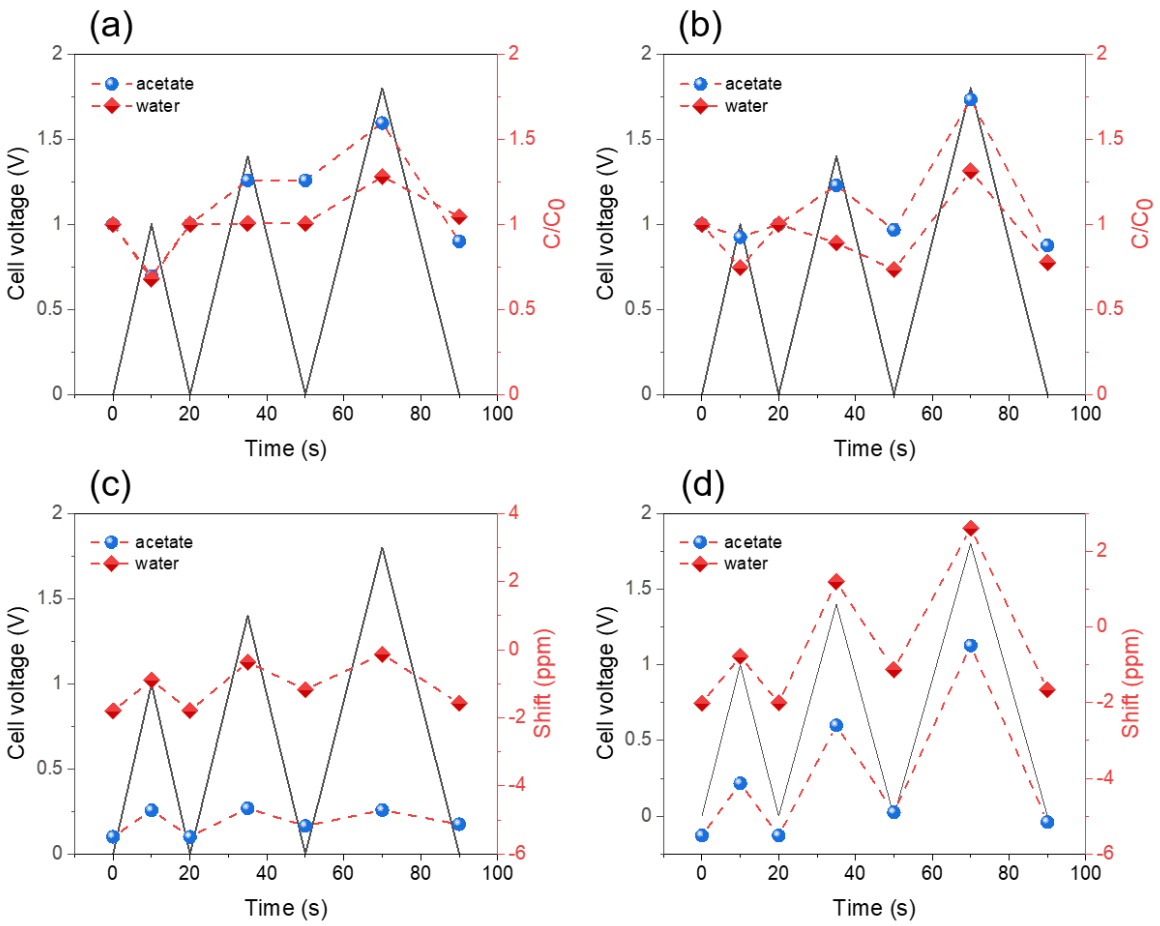

Figure 7. The relative concentrations of acetate ions and water inside the electrode pores of a carbon/carbon supercapacitor at different states of charge and discharge (a, b) and their chemical shifts (c, d) in the positive (a, c) and negative electrodes (b, d).

The additional information that can be obtained from these experiments is the behavior during the discharge of the supercapacitor. The results shown in Figures 7a and b indicate that at the positive electrode, we have a slight flux of species that enters/leaves the pores during charge/discharge. This behavior can be explained by the strong ion-ion and ion-water interactions in the SIPs, which leads to limited mobility for the electrolyte species, with the charge compensation mechanism based on the reorganization of the electrolyte structure in the pores during the charge/discharge of the supercapacitor. A flux of species entering/leaving the pores is only observed at sufficiently high potentials. This explains the increase in the

Corresponding authors: raymundo@cnrs-orleans.fr, michael.deschamps@cnrs-orleans.fr

supercapacitor resistance and the slight decrease in the rate capability observed for increasing electrolyte concentration (Figures S6 and S2a).

For the negative electrode, if one only looks at the cell charged state (values at 1.0 V, 1.4 V and 1.8 V in Figures 7b and d), we obtain the same results (shown above) for the negatively polarized carbon (Figures 5d and e), i.e., an increase in the relative concentrations and shifts for water and acetate for increasing cell voltage. This indicates that from a cell voltage of 1.0 V, the negative electrode already goes through a charge mechanism involving co-ion adsorption of acetate, K^+ and water, i.e., an adsorption of SIPs. From the shift variation, we conclude again that these SIPs are organized in the pores with the K^+ located closer to the surface of the carbon, and water and acetate placed in a second layer.

Although for the case of the positive electrode, we observed that a structuration of the electrolyte into SIPs reduces its mobility inside the carbon pores, we do not observe the same behavior at the negative electrode. Figure 7b shows that the concentrations of water and acetate strongly change during charging and discharging. Moreover, the shifts for the two species vary according to re-entry/exit during charging/discharging (Figure 7d).

These results indicate that the orientation and packing of SIPs inside the carbon pores have an important effect on their diffusion and pore access during charging. If the SIPs are oriented with the acetate located closest to the carbon surface (Scheme 1), the K^+ ions placed at the outer part of the double layer with some surrounding water molecules will limit the entry of new SIPs during the polarization of the positive electrode. However, if the SIPs are oriented with the K^+ ions located closest to the carbon surface (see Scheme 1), the acetate ion placed at the outer part of the double layer having a negative charge closer to the water molecules between the ions will not impede the entry of new SIPs during the polarization of the negative electrode. This can explain the fact that the capacitance of the negative electrode is higher than that of the positive electrode in the WISE-based supercapacitors (Figure 4b and

Corresponding authors: raymundo@cnrs-orleans.fr, michael.deschamps@cnrs-orleans.fr

Figure S3).

These results indicate that for the case of a WISE, it is preferable to have a larger pore size than that found in carbon A to favor the accessibility and mobility of the SIPs at the positive electrode.

3.6 Optimization of the system by an asymmetric carbon configuration

Considering the information obtained above, we chose carbon B with the same specific surface area and amount of oxygen functionalities compared to carbon A but having a wider pore size distribution with more large micropores in the range of 1-2 nm (Table S1 and Figure S7). The cyclic voltammetry presented in Figure 8 shows the important influence of the pore size on the electrochemical behavior of the carbon when using a WISE at 25 mol kg^{-1}. From the potential window over which the positive electrode operates in the supercapacitor (Figure 8a), we confirm that increasing the pore size enables the storage of more SIPs and increases the capacitance. Moreover, if the total stability window of the carbon is explored, Figure 8b shows that the pore size has an even greater influence on the pseudofaradaic processes arising when decreasing the potential down to the water reduction potential. Therefore, the capacitance of the negative electrode of the supercapacitor will also be improved.

Corresponding authors: raymundo@cnrs-orleans.fr, michael.deschamps@cnrs-orleans.fr

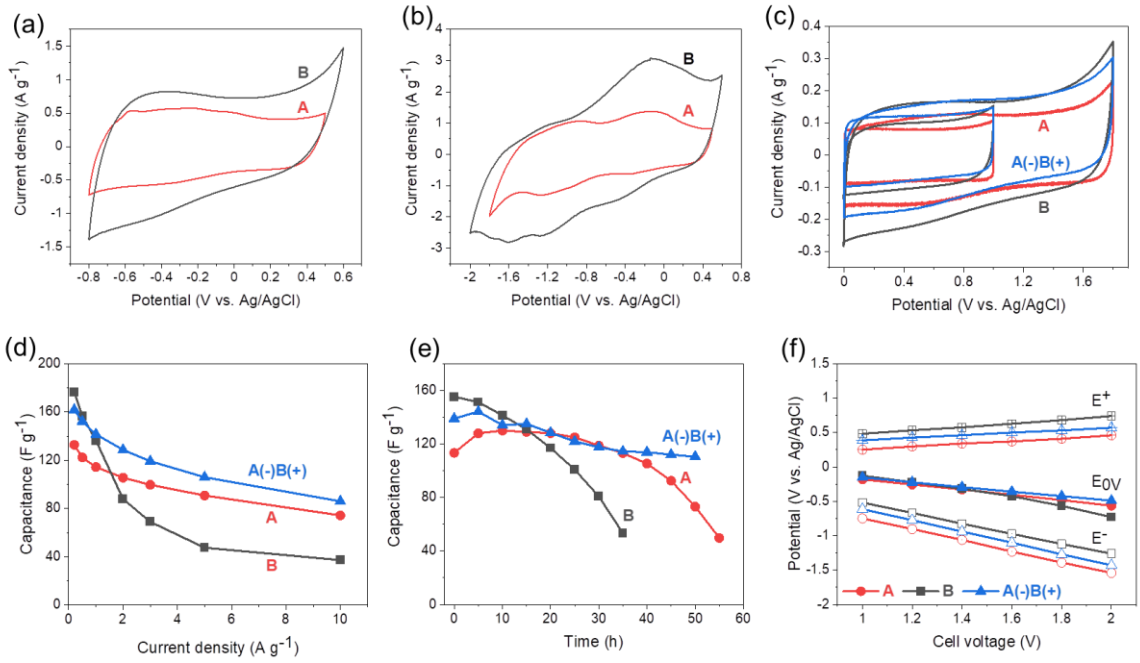

Figure 8. Cyclic voltammetry curves measured at a scan rate of 5 mV s^{-1} for carbon A and carbon B in 25 mol kg^{-1} KAc electrolyte over the operating potential window for the positive electrode in the supercapacitor (a) and in the total stability window for the carbons (b). Carbon/carbon supercapacitors with different electrode configurations using a KAc electrolyte concentration of 25 mol kg^{-1}: cyclic voltammetry curves measured for at a scan rate of 2 mV s^{-1} (c), the rate capability (d), capacitance retention over floating time (e) and potentials of the positive (E^+) and negative electrodes (E^-) at different cell voltages and their potentials when discharging the cells to 0.0 V (E_{0V}) (f).

In fact, the cyclic voltammogram performed over the symmetric carbon/carbon supercapacitors (Figure 8c) confirms that the capacitance of the system with carbon B is higher than that with carbon A. However, the fact that the negative electrode now operates with a large contribution of pseudofaradaic reactions has a negative influence, first on the rate capability (Figure 8d) and second on the supercapacitor cycle life (Figure 8e). Figure 8f shows that carbon B shows a more asymmetric behavior in terms of the capacitance of the two electrodes than carbon A. The negative electrode of carbon B-based supercapacitors has a

Corresponding authors: raymundo@cnrs-orleans.fr, michael.deschamps@cnrs-orleans.fr

much higher capacitance than the positive electrode, driving the latter to operate over a very large potential window beyond the stability window of carbon.

Therefore, since increasing the pore size has the desired effect on the capacitance of the positive electrode, we built an asymmetric system with carbon B for the positive electrode and carbon A for the negative electrode to limit pseudofaradaic contributions. Figure 8 confirms that the asymmetric system presents a higher capacitance than the symmetric system with carbon A (Figures 8c and d) and that the presence of carbon B does not have a negative effect on the rate capability (Figure 8e). As a consequence, for the same cell voltage, the asymmetric configuration allows to store around 25 % more energy at the same time that more power can be extracted at high energy (see Ragone plot in Figure S8). Figure 8e shows that such an asymmetric configuration also leads to an improvement in the cycle life of the supercapacitor as both carbons now operate in their respective stability potential windows (Figure 8f). Therefore the asymmetric configuration can operate at a higher cell voltage to increase the amount of energy stored.

4. CONCLUSIONS

KAc-based concentrated electrolytes are a promising low-cost and environmentally friendly alternative to organic electrolytes used today in the supercapacitor industry. AcK is an inexpensive salt with high solubility, which allows for a low-cost WISE without the presence of fluorine, as is the case for the more widely studied and more expensive LiTFSI-based WISEs. KAc WISE enables carbon/carbon supercapacitors to operate at higher cell voltages than dilute aqueous electrolytes. By carrying out *operando* PEMS, we confirmed that the main cause of aging in our diluted aqueous-based supercapacitors is the oxidation of the positive electrode and show how increasing the concentration of the electrolyte enables one to decrease the extent of these irreversible reactions, and, therefore, to operate the supercapacitor

Corresponding authors: raymundo@cnrs-orleans.fr, michael.deschamps@cnrs-orleans.fr

at a higher cell voltage.

A detailed investigation of the carbon/electrolyte interface based on combining electrochemical measurements with Raman spectroscopy, mass spectrometry and NMR sheds new light on the effect of electrolyte concentration on the charge/discharge mechanism for a supercapacitor. Raman experiments for the electrolytes confirm that increasing the concentration drives the transformation from an electrolyte with water-solvated, independent ions to an electrolyte with solvent-separated ion pairs (SIPs). Therefore, the mechanism of charge storage evolves from ion exchange at low concentrations to ion coadsorption and/or rearrangement of SIPs inside the carbon pores for a WISE. NMR results show that the structure of the electrolyte also impacts the way the electrolyte is oriented within the electrode pores, influencing the mobility of ions in the pores of the electrodes differently for the case of the positive and the negative electrodes during the charging and discharging of the supercapacitor.

The information obtained from a combination of the above-mentioned experimental techniques for the structure of the electrolyte and the charge storage mechanism paves the way to improve the performance of our WISE-based supercapacitors, better adapting the porosity of the electrode materials to the charging mechanism for each electrode in an asymmetric configuration.

SUPPORTING INFORMATON

Gases produced inside the supercapacitors after 30 hours of floating; pressures inside the supercapacitors as a function of floating time; capacitance retention as a function of current density; Ragone plot comparing a carbon/carbon supercapacitors built with the KAc electrolyte at 25 mol kg^{-1} operating at 2.0 V to a carbon/carbon supercapacitor built with a 21 mol kg^{-1} LiTFSI electrolyte operating at 2.4 V; ^{1}H NMR spectra of 5 mol kg^{-1} KAc electrolyte

Corresponding authors: raymundo@cnrs-orleans.fr, michael.deschamps@cnrs-orleans.fr

and of carbon A impregnated in the 5 mol kg^{-1} KAc electrolyte; υC-C stretching modes and υ_sC-O modes from Raman spectra of KAc solutions; Nyquist plots, capacitance retention as a function of current density and resistances compared to the conductivity of the electrolytes; specific surface areas, pore size distributions and oxygen contents of carbon A and carbon B.

ACKNOWLEDGEMENTS

ERP, MD, CN and RO thank the French National Research Agency (STORE-EX Labex Project ANR-10-LABX-76-01) and ERP, RO, HP thank the Région Centre val de Loire (Project APR-IA PRESERVE convention n°2019 00134933) for financial support.

REFERENCES

(1) Suo, L.; Borodin, O.; Gao, T.; Olguin, M.; Ho, J.; Fan, X.; Luo, C.; Wang, C.; Xu, K. "Water-in-Salt" Electrolyte Enables High-Voltage Aqueous Lithium-Ion Chemistries. *Science (80-.).* **2015**, *350* (6263), 938–943. https://doi.org/10.1126/science.aab1595.

(2) Lannelongue, P.; Bouchal, R.; Mourad, E.; Bodin, C.; Olarte, M.; le Vot, S.; Favier, F.; Fontaine, O. "Water-in-Salt" for Supercapacitors: A Compromise between Voltage, Power Density, Energy Density and Stability. *J. Electrochem. Soc.* **2018**, *165* (3), A657–A663. https://doi.org/10.1149/2.0951803jes.

(3) Dou, Q.; Lei, S.; Wang, D. W.; Zhang, Q.; Xiao, D.; Guo, H.; Wang, A.; Yang, H.; Li, Y.; Shi, S.; Yan, X. Safe and High-Rate Supercapacitors Based on an "Acetonitrile/Water in Salt" Hybrid Electrolyte. *Energy Environ. Sci.* **2018**, *11* (11), 3212–3219. https://doi.org/10.1039/c8ee01040d.

(4) Liu, X.; Mi, R.; Yuan, L.; Yang, F.; Fu, Z.; Wang, C.; Tang, Y. Nitrogen-Doped Multi-Scale Porous Carbon for High Voltage Aqueous Supercapacitors. *Front. Chem.* **2018**, *6* (OCT), 1–10. https://doi.org/10.3389/fchem.2018.00475.

Corresponding authors: raymundo@cnrs-orleans.fr, michael.deschamps@cnrs-orleans.fr

(5) McEldrew, M.; Goodwin, Z. A. H.; Kornyshev, A. A.; Bazant, M. Z. Theory of the Double Layer in Water-in-Salt Electrolytes. *J. Phys. Chem. Lett.* **2018**, *9* (19), 5840–5846. https://doi.org/10.1021/acs.jpclett.8b02543.

(6) Amiri, M.; Bélanger, D. Physicochemical and Electrochemical Properties of Water-in-Salt Electrolytes. *ChemSusChem* **2021**, *14* (12), 2487–2500. https://doi.org/10.1002/cssc.202100550.

(7) Bu, X.; Su, L.; Dou, Q.; Lei, S.; Yan, X. A Low-Cost "Water-in-Salt" Electrolyte for a 2.3 V High-Rate Carbon-Based Supercapacitor. *J. Mater. Chem. A* **2019**, *7* (13), 7541–7547. https://doi.org/10.1039/c9ta00154a.

(8) Tian, X.; Zhu, Q.; Xu, B. "Water-in-Salt" Electrolytes for Supercapacitors: A Review. *ChemSusChem* **2021**, *14* (12), 2501–2515. https://doi.org/10.1002/cssc.202100230.

(9) Lu, X.; Vicent-Luna, J. M.; Calero, S.; Madero-Castro, R. M.; Gutiérrez, M. C.; Ferrer, M. L.; del Monte, F. EMIMBF4 in Ternary Liquid Mixtures of Water, Dimethyl Sulfoxide and Acetonitrile as "Tri-Solvent-in-Salt" Electrolytes for High-Performance Supercapacitors Operating at -70 °C. *Energy Storage Mater.* **2021**, *40* (April), 368–385. https://doi.org/10.1016/j.ensm.2021.05.026.

(10) Guo, J.; Ma, Y.; Zhao, K.; Wang, Y.; Yang, B.; Cui, J.; Yan, X. High-Performance and Ultra-Stable Aqueous Supercapacitors Based on a Green and Low-Cost Water-In-Salt Electrolyte. *ChemElectroChem* **2019**, *6* (21), 5433–5438. https://doi.org/10.1002/celc.201901591.

(11) Galek, P.; Frackowiak, E.; Fic, K. Interfacial Aspects Induced by Saturated Aqueous Electrolytes in Electrochemical Capacitor Applications. *Electrochim. Acta* **2020**, *334*, 135572. https://doi.org/10.1016/j.electacta.2019.135572.

(12) Tian, Z.; Deng, W.; Wang, X.; Liu, C.; Li, C.; Chen, J.; Xue, M.; Li, R.; Pan, F. Superconcentrated Aqueous Electrolyte to Enhance Energy Density for Advanced

Supercapacitors. *Funct. Mater. Lett.* **2017**, *10* (6), 1–5. https://doi.org/10.1142/S1793604717500813.

(13) Merlet, C.; Rotenberg, B.; Madden, P. A.; Taberna, P. L.; Simon, P.; Gogotsi, Y.; Salanne, M. On the Molecular Origin of Supercapacitance in Nanoporous Carbon Electrodes. *Nat. Mater.* **2012**, *11* (4), 306–310. https://doi.org/10.1038/nmat3260.

(14) Merlet, C.; Péan, C.; Rotenberg, B.; Madden, P. A.; Daffos, B.; Taberna, P. L.; Simon, P.; Salanne, M. Highly Confined Ions Store Charge More Efficiently in Supercapacitors. *Nat. Commun.* **2013**, *4* (May), 2–7. https://doi.org/10.1038/ncomms3701.

(15) Jiang, D. E.; Jin, Z.; Henderson, D.; Wu, J. Solvent Effect on the Pore-Size Dependence of an Organic Electrolyte Supercapacitor. *J. Phys. Chem. Lett.* **2012**, *3* (13), 1727–1731. https://doi.org/10.1021/jz3004624.

(16) Levi, M. D.; Sigalov, S.; Salitra, G.; Aurbach, D.; Maier, J. The Effect of Specific Adsorption of Cations and Their Size on the Charge-Compensation Mechanism in Carbon Micropores: The Role of Anion Desorption. *ChemPhysChem* **2011**, *12* (4), 854–862. https://doi.org/10.1002/cphc.201000653.

(17) Deschamps, M.; Gilbert, E.; Azais, P.; Raymundo-Piñero, E.; Ammar, M. R.; Simon, P.; Massiot, D.; Béguin, F. Exploring Electrolyte Organization in Supercapacitor Electrodes with Solid-State NMR. *Nat. Mater.* **2013**, *12* (4), 351–358. https://doi.org/10.1038/nmat3567.

(18) Oukali, G.; Salager, E.; Ammar, M. R.; Dutoit, C. E.; Sarou-Kanian, V.; Simon, P.; Raymundo-Piñero, E.; Deschamps, M. In Situ Magnetic Resonance Imaging of a Complete Supercapacitor Giving Additional Insight on the Role of Nanopores. *ACS Nano* **2019**, *13* (11), 12810–12815. https://doi.org/10.1021/acsnano.9b04998.

(19) Feng, G.; Jiang, X.; Qiao, R.; Kornyshev, A. A. Water in Ionic Liquids at Electrified

Corresponding authors: raymundo@cnrs-orleans.fr, michael.deschamps@cnrs-orleans.fr

Interfaces: The Anatomy of Electrosorption. *ACS Nano* **2014**, *8* (11), 11685–11694. https://doi.org/10.1021/nn505017c.

(20) Groves, T. S.; Perez-Martinez, C. S.; Lhermerout, R.; Perkin, S. Surface Forces and Structure in a Water-in-Salt Electrolyte. *J. Phys. Chem. Lett.* **2021**, *12* (6), 1702–1707. https://doi.org/10.1021/acs.jpclett.0c03718.

(21) Lin, R.; Taberna, P.-L.; Fantini, S.; Presser, V.; Pérez, C. R.; Malbosc, F.; Rupesinghe, N. L.; Teo, K. B. K.; Gogotsi, Y.; Simon, P. Capacitive Energy Storage from −50 to 100 °C Using an Ionic Liquid Electrolyte. *J. Phys. Chem. Lett.* **2011**, *2* (19), 2396–2401. https://doi.org/10.1021/jz201065t.

(22) Lewis, N. H. C.; Zhang, Y.; Dereka, B.; Carino, E. V.; Maginn, E. J.; Tokmakoff, A. Signatures of Ion Pairing and Aggregation in the Vibrational Spectroscopy of Super-Concentrated Aqueous Lithium Bistriflimide Solutions. *J. Phys. Chem. C* **2020**, *124* (6), 3470–3481. https://doi.org/10.1021/acs.jpcc.9b10477.

(23) Miyazaki, K.; Takenaka, N.; Watanabe, E.; Iizuka, S.; Yamada, Y.; Tateyama, Y.; Yamada, A. First-Principles Study on the Peculiar Water Environment in a Hydrate-Melt Electrolyte. *J. Phys. Chem. Lett.* **2019**, *10* (20), 6301–6305. https://doi.org/10.1021/acs.jpclett.9b02207.

(24) Li, Z.; Jeanmairet, G.; Méndez-Morales, T.; Rotenberg, B.; Salanne, M. Capacitive Performance of Water-in-Salt Electrolytes in Supercapacitors: A Simulation Study. *J. Phys. Chem. C* **2018**, *122* (42), 23917–23924. https://doi.org/10.1021/acs.jpcc.8b07557.

(25) Batisse, N.; Raymundo-Piñero, E. Pulsed Electrochemical Mass Spectrometry for Operando Tracking of Interfacial Processes in Small-Time-Constant Electrochemical Devices Such as Supercapacitors. *ACS Appl. Mater. Interfaces* **2017**, *9* (47), 41224–41232. https://doi.org/10.1021/acsami.7b12068.

Corresponding authors: raymundo@cnrs-orleans.fr, michael.deschamps@cnrs-orleans.fr

(26) Massiot, D.; Fayon, F.; Capron, M.; King, I.; Le Calvé, S.; Alonso, B.; Durand, J. O.; Bujoli, B.; Gan, Z.; Hoatson, G. Modelling One- and Two-Dimensional Solid-State NMR Spectra. *Magn. Reson. Chem.* **2002**, *40* (1), 70–76. https://doi.org/10.1002/mrc.984.

(27) Demarconnay, L.; Raymundo-Piñero, E.; Béguin, F. A Symmetric Carbon/Carbon Supercapacitor Operating at 1.6 V by Using a Neutral Aqueous Solution. *Electrochem. commun.* **2010**, *12* (10), 1275–1278. https://doi.org/10.1016/j.elecom.2010.06.036.

(28) Fic, K.; Lota, G.; Meller, M.; Frackowiak, E. Novel Insight into Neutral Medium as Electrolyte for High-Voltage Supercapacitors. *Energy Environ. Sci.* **2012**, *5* (2), 5842–5850. https://doi.org/10.1039/c1ee02262h.

(29) Gao, Q.; Demarconnay, L.; Raymundo-Piñero, E.; Béguin, F. Exploring the Large Voltage Range of Carbon/Carbon Supercapacitors in Aqueous Lithium Sulfate Electrolyte. *Energy Environ. Sci.* **2012**, *5* (11), 9611–9617. https://doi.org/10.1039/c2ee22284a.

(30) Jurewicz, K.; Frackowiak, E.; Béguin, F. Towards the Mechanism of Electrochemical Hydrogen Storage in Nanostructured Carbon Materials. *Appl. Phys. A Mater. Sci. Process.* **2004**, *78* (7), 981–987. https://doi.org/10.1007/s00339-003-2418-8.

(31) Béguin, F.; Friebe, M.; Jurewicz, K.; Vix-Guterl, C.; Dentzer, J.; Frackowiak, E. State of Hydrogen Electrochemically Stored Using Nanoporous Carbons as Negative Electrode Materials in an Aqueous Medium. *Carbon N. Y.* **2006**, *44* (12), 2392–2398. https://doi.org/10.1016/j.carbon.2006.05.025.

(32) Xu, S. W.; Zhang, M. C.; Zhang, G. Q.; Liu, J. H.; Liu, X. Z.; Zhang, X.; Zhao, D. D.; Xu, C. L.; Zhao, Y. Q. Temperature-Dependent Performance of Carbon-Based Supercapacitors with Water-in-Salt Electrolyte. *J. Power Sources* **2019**, *441* (September), 227220. https://doi.org/10.1016/j.jpowsour.2019.227220.

Corresponding authors: raymundo@cnrs-orleans.fr, michael.deschamps@cnrs-orleans.fr

(33) Forse, A. C.; Griffin, J. M.; Presser, V.; Gogotsi, Y.; Grey, C. P. Ring Current Effects: Factors Affecting the NMR Chemical Shift of Molecules Adsorbed on Porous Carbons. *J. Phys. Chem. C* **2014**, *118* (14), 7508–7514. https://doi.org/10.1021/jp502387x.

(34) Han, J.; Mariani, A.; Zhang, H.; Zarrabeitia, M.; Gao, X.; Carvalho, D. V.; Varzi, A.; Passerini, S. Gelified Acetate-Based Water-in-Salt Electrolyte Stabilizing Hexacyanoferrate Cathode for Aqueous Potassium-Ion Batteries. *Energy Storage Mater.* **2020**, *30*, 196–205. https://doi.org/10.1016/j.ensm.2020.04.028.

(35) Rudolph, W. W.; Fischer, D.; Irmer, G. Vibrational Spectroscopic Studies and DFT Calculations on $NaCH_3CO_2$(aq) and CH_3COOH(aq). *Dalt. Trans.* **2014**, *43* (8), 3174–3185. https://doi.org/10.1039/c3dt52580e.

(36) De Oliveira, D. M.; Zukowski, S. R.; Palivec, V.; Hénin, J.; Martinez-Seara, H.; Ben-Amotz, D.; Jungwirth, P.; Duboué-Dijon, E. Binding of Divalent Cations to Acetate: Molecular Simulations Guided by Raman Spectroscopy. *Phys. Chem. Chem. Phys.* **2020**, *22* (41), 24014–24027. https://doi.org/10.1039/d0cp02987d.

(37) Wahab, A.; Mahiuddin, S.; Hefter, G.; Kunz, W.; Minofar, B.; Jungwirth, P. Ultrasonic Velocities, Densities, Viscosities, Electrical Conductivities, Raman Spectra, and Molecular Dynamics Simulations of Aqueous Solutions of $Mg(OAc)_2$ and $Mg(NO_3)_2$: Hofmeister Effects and Ion Pair Formation. *J. Phys. Chem. B* **2005**, *109* (50), 24108–24120. https://doi.org/10.1021/jp053344q.

(38) Chang, T. G.; Irish, D. E. Raman and Infrared Spectral Study of Magnesium Nitrate-Water Systems. *J. Phys. Chem.* **1973**, *77* (1), 52–57. https://doi.org/10.1021/j100620a011.

Corresponding authors: raymundo@cnrs-orleans.fr, michael.deschamps@cnrs-orleans.fr

Table of contents

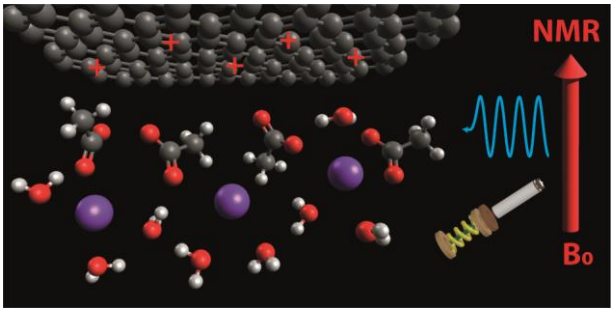

A detailed investigation of the carbon/electrolyte interface based on combining electrochemical measurements with Raman spectroscopy, mass spectrometry and NMR sheds new light on the effect of electrolyte concentration on the charge/discharge mechanism for a supercapacitor. The information obtained for the structure of the electrolyte and the charge storage mechanism paves the way to improve the performance of WISE-based supercapacitors by optimizing the physicochemical-properties of the electrode materials.

Corresponding authors: raymundo@cnrs-orleans.fr, michael.deschamps@cnrs-orleans.fr